

# Dynamics and control of a MEMS angle measuring gyroscope

Sungsu Park<sup>a,\*</sup>, Roberto Horowitz<sup>b</sup>, Chin-Woo Tan<sup>c</sup>

<sup>a</sup> Department of Aerospace Engineering, Sejong University, 98 Gunja-dong, Kwangjin-gu, Seoul, Republic of Korea

<sup>b</sup> Department of Mechanical Engineering, University of California at Berkeley, Berkeley, CA 94720, United States

<sup>c</sup> PATH, University of California at Berkeley, Richmond, CA 94804, United States

Received 17 March 2007; received in revised form 14 November 2007; accepted 31 December 2007

Available online 17 January 2008

## Abstract

This paper presents an algorithm for controlling vibratory MEMS gyroscopes so that they can directly measure the rotation angle without integration of the angular rate, thus eliminating the accumulation of numerical integration errors incurred in obtaining the angle from the angular rate. The proposed control algorithm consists of a weighted energy control and a mode tuning control. The weighed energy control compensates unequal damping terms and keeps the amplitude of oscillation constant in an inertial frame by maintaining the prescribed total energy. The mode tuning control continuously tunes mismatches in spring stiffness in order to maintain a straight line of oscillation for the proof mass. The simulation results demonstrate the feasibility of the control algorithm and the viability of the concept of using a vibratory gyroscope to directly measure rotation angle.

© 2008 Elsevier B.V. All rights reserved.

**Keywords:** Angle measurement; MEMS gyroscope; Energy control; Mode tuning

## 1. Introduction

MEMS gyroscopes are typically angular rate gyroscopes that are designed to measure the angular rate [1]. In order to obtain the rotation angle using a MEMS rate gyroscope, it is required to integrate the measured angular rate with respect to time. The integration process, however, causes the rotation angle to drift over time and therefore the angle error to diverge quickly due to the presence of bias and noise in the angular rate signal. These effects are more severe for low cost MEMS rate gyroscopes.

Several techniques have been proposed and commercialized to bound the error divergence resulted from the integration of gyroscope angular rate signal. The most common technique is to fuse rate gyroscopes with accelerometers and magnetometers based on the fact that steady-state pitch and roll angles can be obtained using accelerometers, and yaw angles can be obtained using magnetometers. This technique, however, has a few drawbacks. The magnetometer signals can be severely distorted by

unwanted magnetic fields in the vicinity of the sensors. The rotation angles can be correctly obtained from accelerometer measurements only when the moving object is in steady state. Moreover, yaw angle cannot be obtained using accelerometers, although there are a number of applications where yaw angle must be measured correctly such as automobile and home robot navigation [2].

MEMS gyroscopes can conceptually operate in the rotation angle measurement mode. When an isotropic oscillator is allowed to freely oscillate, the precession of the angle of rotation. For freely oscillating, the natural frequencies of oscillation of the two vibrating modes must be the same and the modes are undamped. Ideally, the vibrating modes of a MEMS gyroscope are supposed to remain mechanically decoupled, their natural frequencies should be matched, and the output of the gyroscope should be sensitive to only rotation. In practice, however, fabrication defects and environment variations are always present, resulting in a mismatch of the frequencies of oscillation for the two vibrating modes and the presence of linear dissipative forces with damping coefficients [3]. These fabrication imperfections are major factors that limit realization of an angle measuring gyroscope. Although most published control algorithms deal with rate gyroscope [4–6], a few control algorithms for real-

\* Corresponding author. Tel.: +82 2 3408 3769; fax: +82 2 3408 3333.

E-mail addresses: [sungsu@sejong.ac.kr](mailto:sungsu@sejong.ac.kr) (S. Park), [horowitz@me.berkeley.edu](mailto:horowitz@me.berkeley.edu) (R. Horowitz), [tan@eecs.berkeley.edu](mailto:tan@eecs.berkeley.edu) (C.-W. Tan).

izing angle measuring gyroscopes have been presented in Refs. [7–12]. Friedland and Hutton [7] suggested the use of a vibratory gyroscope for measuring rotation angle. A composite nonlinear feedback control is reported in Refs. [8–11], where the energy control and angular momentum control are developed based on the analytic results of Ref. [7]. However, their energy control relies on the equal damping assumption, and the angular momentum control is vulnerable to interference with the Coriolis acceleration. Another composite nonlinear feedback control is proposed in Ref. [12], where the stability of the controlled system is not proven.

In this paper, we present a new control algorithm for realizing angle measuring gyroscopes. The developed control algorithm maintains the prescribed total energy level, and compensates for mismatched stiffness and damping, so as to ensure that the proof mass maintains a straight line of oscillation and keeps the magnitude of amplitude in the inertial frame.

## 2. Dynamics of a vibratory angle measuring gyroscope

The equation of motion of a mass freely oscillating in two degrees-of-freedom (2-DOF) at frequency  $\omega_0$  in an inertial frame is given by

$$\ddot{q}_i + \omega_0^2 q_i = 0 \quad (1)$$

where  $q_i = [x_i \ y_i]^T$  is displacement of mass along the  $\hat{e}_1$  and  $\hat{e}_2$  axis of the inertial frame. To describe the motion of a mass freely oscillating in the gyro frame, which rotates about the  $\hat{e}_3$  axis of the inertial frame, a coordinate transformation is performed using the relation:

$$q_i = C_g^i q \quad (2)$$

where  $C_g^i = \begin{bmatrix} \cos \psi & -\sin \psi \\ \sin \psi & \cos \psi \end{bmatrix}$  is the direction cosine matrix,  $\psi$  is the rotation angle, and  $q = [xy]^T$  is displacement vector along the  $\hat{g}_1$  and  $\hat{g}_2$  axes of the gyro frame.

If Eq. (2) is substituted to Eq. (1), then we get

$$\ddot{q} + [\dot{\omega}_{ig}^g \times] q + 2[\omega_{ig}^g \times] \dot{q} + (\omega_0^2 - \dot{\psi}^2) q = 0 \quad (3)$$

where  $[\omega_{ig}^g \times] = \begin{bmatrix} 0 & -\dot{\psi} \\ \dot{\psi} & 0 \end{bmatrix}$  is the angular rate matrix of the gyro frame with respect to the inertial frame.

If the line of oscillation of the mass with amplitude  $M$  is aligned with the  $\hat{e}_1$  axis, then the solution of Eq. (3) is given by

$$\begin{aligned} x &= M \cos(\dot{\psi} t) \sin(\omega_0 t) \\ y &= -M \sin(\dot{\psi} t) \sin(\omega_0 t) \end{aligned} \quad (4)$$

Eq. (3) is approximated as following equation with the assumption that  $\omega_0 \gg \dot{\psi}$  and  $\dot{\psi} \approx 0$ .

$$\begin{aligned} \ddot{x} + \omega_0^2 x &= 2\dot{\psi} \dot{y} \\ \ddot{y} + \omega_0^2 y &= -2\dot{\psi} \dot{x} \end{aligned} \quad (5)$$

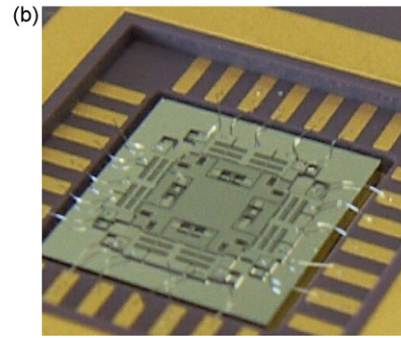
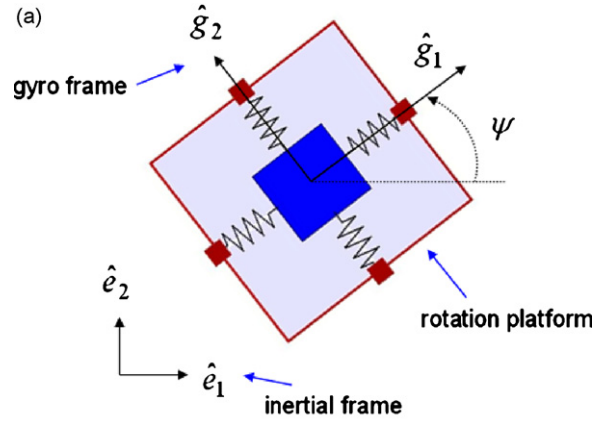


Fig. 1. MEMS gyroscope: (a) model and (b) gyroscope fabricated by Sejong University.

Eq. (5) describes the motion of 2-DOF freely oscillating mass with frequency  $\omega_0$  in the gyro frame. The rotation angle  $\psi$  can be calculated with Eq. (4) by measuring displacement  $x$  and  $y$  in the gyro frame. Therefore, Eq. (5) is referred to as the dynamics of an ideal vibratory angle measuring gyroscope.

A physical angle measuring gyroscope can be implemented by the 2-DOF mass-spring-damper system whose proof mass is suspended by spring flexure anchored at the gyro frame, as shown in Fig. 1. A vibratory angle measuring gyroscope has the same structure as a vibratory rate gyroscope, and there are reports of various types of rate gyroscopes in the literature and industry.

Considering fabrication imperfections and damping, a realistic model of a z-axis gyroscope is described as follows:

$$\begin{aligned} \ddot{x} + d_x \dot{x} + \omega_x^2 x + \omega_{xy} y &= f_x + 2\dot{\psi} \dot{y} \\ \ddot{y} + d_y \dot{y} + \omega_y^2 y + \omega_{xy} x &= f_y - 2\dot{\psi} \dot{x} \end{aligned} \quad (6)$$

where  $d_x$  and  $d_y$  are damping,  $\omega_x$  and  $\omega_y$  are natural frequencies of the  $x$ - and  $y$ -axis,  $\omega_{xy}$  is a coupled frequency term, and  $f_x$  and  $f_y$  are the specific control forces applied to the proof mass in  $\hat{g}_1$  and  $\hat{g}_2$  axis of the gyro frame, respectively. The coupled frequency term, called quadrature error, comes mainly from asymmetries in suspension structure and misalignment of sensors and actuators. Recently, a mechanically decoupled gyroscope structure has been proposed in the literature and it is shown that two axes can be mechanically decoupled to a great extent by using a unidirectional frame structure [13,14].

### 3. Design of control algorithm

The control problem of angle measuring gyroscope is formalized as follows; given the realistic gyroscope model,

$$\ddot{q} + \omega_0^2 q = f - D\dot{q} - Rq - 2[\omega_{ig}^s \times]q \quad (7)$$

where  $f = [f_x \ f_y]^T$ ,  $D = \begin{bmatrix} d_x & 0 \\ 0 & d_y \end{bmatrix}$ ,  $R = \begin{bmatrix} \Delta\omega_x & 0 \\ 0 & \Delta\omega_y \end{bmatrix}$  and  $\Delta\omega_x = \omega_x^2 - \omega_0^2$ ,  $\Delta\omega_y = \omega_y^2 - \omega_0^2$ , determine the control laws for  $f_x$  and  $f_y$ , such that the damping terms,  $d_x$  and  $d_y$ , and mismatches in natural frequencies,  $\Delta\omega_x$  and  $\Delta\omega_y$ , are correctly compensated for the realistic gyroscope to be operated as an ideal angle measuring gyroscope. Note that the gyroscope operates at a fixed frequency,  $\omega_0$ , which is chosen by the designer. In such a way, natural frequencies of both axes can be actively tuned to be matched, and the associated signal processing can be simplified as well.

In this section, we propose an adaptive controller to compensate for damping terms and mismatches in natural frequencies by performing two tasks: (a) initiating oscillation and maintaining total energy level, and (b) tuning any mismatch in the natural frequencies of both axes.

#### 3.1. Weighted energy control

When the gyroscope rotates, the line of oscillation precesses because the Coriolis acceleration transfers energy between the two axes of the gyroscope, while conserving the total energy of the gyroscope. This can be shown by defining the instantaneous total mechanical energy  $E$  as

$$E = \frac{1}{2}(\dot{q}^T \dot{q} + \omega_0^2 q^T q) \quad (8)$$

and differentiating it along the trajectory of an ideal gyroscope (5) as follows.

$$\dot{E} = \dot{q}^T \ddot{q} + \omega_0^2 \dot{q}^T q = \dot{q}^T (-\omega_0^2 q - 2[\omega_{ig}^s \times] \dot{q}) + \omega_0^2 \dot{q}^T q = 0 \quad (9)$$

From Eq. (9), it is clear that the angular rate term does not change the total energy. However, in case of a non-ideal gyroscope, the total energy is not conserved because of the damping terms.

Therefore, the purpose of an energy control should be to maintain the prescribed energy level so that the damping is compensated without interference with the angular rate, and also to excite the proof mass into oscillation. If the prescribed energy level is larger than the current energy level, then the magnitude of energy control is chosen to be positive for growing the oscillation, and conversely negative for damping the oscillation. In such a way, the magnitude of energy control effectively compensates the damping terms and sustains free oscillation of the system.

The deviation of actual energy level of the system from the prescribed one is defined by

$$\tilde{E} = E_0 - \frac{1}{2}(\dot{q}^T \dot{q} + \omega_0^2 q^T q) \quad (10)$$

where  $E_0$  denotes the prescribed energy level. Note that total energy is computed based on the designed reference frequency  $\omega_0$ . Now, consider the following positive definite function (PDF).

$$V = \frac{1}{2} \left( \tilde{E}^2 + \frac{1}{K_1} \text{tr}\{\tilde{D}\tilde{D}^T\} \right) \quad (11)$$

where  $K_1$  is a positive constant,  $\tilde{D} = \hat{D} - D$  where  $\hat{D}$  is the estimate of  $D$ , and  $\text{tr}\{\cdot\}$  denotes the trace of the matrix. The derivative of the PDF  $V$  along the trajectory of Eq. (7) is

$$\dot{V} = \tilde{E}\dot{\tilde{E}} + \frac{1}{K_1} \text{tr}\{\tilde{D}\dot{\tilde{D}}^T\} \quad (12)$$

If the energy control law  $f_E$  is chosen to be

$$f_E = \hat{D}\dot{q} + f_1 \quad (13)$$

where  $f_1$  is an auxiliary control action that will be defined subsequently, then the derivative of the PDF  $V$  is computed as follows, assuming that the natural frequencies are compensated to be the reference natural frequency.

$$\dot{V} = \tilde{E}(-\dot{q}^T f_1 - \dot{q}^T \tilde{D}\dot{q}) + \frac{1}{K_1} \text{tr}\{\tilde{D}\dot{\tilde{D}}^T\} \quad (14)$$

If  $f_1$  is chosen to be

$$f_1 = K_P \tilde{E}\dot{q} \quad (15)$$

where  $K_P$  is a positive constant, then Eq. (14) becomes:

$$\dot{V} = -K_P \tilde{E}^2 \dot{q}^T \dot{q} + \text{tr} \left\{ \frac{1}{K_1} \tilde{D}\dot{\tilde{D}}^T - \tilde{E}\tilde{D}\dot{q}\dot{q}^T \right\} \quad (16)$$

Eq. (16) suggests the following adaptation law for:

$$\dot{\tilde{D}} = K_1 \tilde{E}\dot{q}\dot{q}^T \quad (17)$$

leads to  $\dot{V} = -K_P \tilde{E}^2 \dot{q}^T \dot{q} \leq 0$ .

**Theorem 1.** With the control laws (13) and (15), and damping adaptation law (17), the following results hold.

- The total energy error  $\tilde{E}$  and its time-derivative both converge to zero as  $t \rightarrow \infty$ .
- The convergence of the damping estimate,  $\hat{D}$ , to its true value is guaranteed only when equal damping of both axes is assumed.

According to **Theorem 1**, the energy control can compensate the damping terms only when both axes have the same damping values. Since unequal damping terms cause different dissipation of energy, different weightings on the total energy control are required. This fact suggests a modification of the energy control law which we summarize in the following theorem.

**Theorem 2.** If the damping ratio of both axes is known, then the total energy error and damping estimate error converge to zero as  $t \rightarrow \infty$  when the following control law (18) and damping adaptation law (19) are applied.

$$f_E = K_P \tilde{E}\dot{q} + \hat{\alpha}\Lambda\dot{q} \quad (18)$$

$$\dot{\hat{\alpha}} = K_I \tilde{E}(\dot{q}^T \Lambda \dot{q}) \quad (19)$$

where  $\Lambda$  is a damping ratio matrix to satisfy  $D=\alpha\Lambda$ ,  $\alpha$  is an associated scalar value,  $\hat{\alpha}$  is the estimate of  $\alpha$ , and  $\tilde{\alpha} = \hat{\alpha} - \alpha$ .

The original energy control is modified using the damping ratio matrix and therefore compensates different dissipation of two axes. The damping ratio can be obtained at an initialization stage which we will explain later.

### 3.2. Mode tuning control

The natural frequencies of the two axes must be matched precisely, but the accuracy required is beyond the manufacturing tolerance. Since the natural frequency changes with temperature and other environment factors, we propose that the fixed reference frequency,  $\omega_0$ , is specified by the designer. Therefore, the purpose of mode tuning control is to track reference frequency by compensating for  $x$ - and  $y$ -axis natural frequency deviations from the reference frequency. The introduction of the concept of reference frequency is very useful since it can simplify signal processing needed for calculating the total energy and demodulating the output signals.

The mode tuning control for both axes is given by

$$f_M = \hat{R}q = \begin{bmatrix} \Delta\hat{\omega}_x x \\ \Delta\hat{\omega}_y y \end{bmatrix} \quad (20)$$

where the frequency deviations are estimated by a frequency deviation estimator. Since both axes share the same mode tuning control scheme, we will explain a frequency deviation estimator for  $x$ -axis only for simplicity. A frequency deviation estimator consists of two function blocks: phase detector and controller.

The phase detector compares the phase difference between the driving signal and the output. Consider an ideal gyroscope behavior and a velocity feedback energy control, the driving signal can be assumed to be  $\cos \omega_0 t$  multiplied by a constant. Therefore, the output of phase detector is the product of the measured position signal and the driving signal,  $\cos \omega_0 t$ , filtered by a low-pass filter, i.e.

$$\tilde{\theta} = \text{LPF}(x \text{sgn}(X) \cos \omega_0 t) \quad (21)$$

where  $\tilde{\theta}$  is the phase difference,  $x$  is the measured position signal, LPF denotes a low-pass filter, and  $\text{sgn}(X)$  is the sign of the measured velocity signal  $\dot{x}$  compared to reference driving signal  $\cos \omega_0 t$ , i.e.

$$X = \text{LPF}(\cos \omega_0 t \dot{x}) \quad (22)$$

The  $x$ -axis frequency deviation,  $\Delta\hat{\omega}_x$ , is calculated from the phase difference,  $\tilde{\theta}$ , by using an integral controller,

$$\Delta\hat{\omega}_x = \frac{K_{IM}}{s} \tilde{\theta} \quad (23)$$

where  $K_{IM}$  is the integral control gain. Stability analysis of this mode tuning control scheme can be obtained in a similar fashion as that in the literature for PLL [16].

### 3.3. Initialization

As mentioned in Theorem 2, the energy control needs a damping ratio matrix  $\Lambda$  to compensate for the different dissipations of two axes. There may be two approaches in identifying this damping ratio matrix. One approach is to drive both axes with the same control such as

$$f_{x,y} = A \cos \omega_0 t \quad (24)$$

where  $A$  is the fixed amplitude of the control. The damping ratio is identified by calculating the energy ratio using the fact that the damping ratio is inversely proportional to the square-root of the energy ratio, i.e.

$$\frac{d_y}{d_x} = \sqrt{\frac{E_X}{E_Y}} \quad (25)$$

where

$$E_X = \frac{1}{2}(\dot{x}^2 + \omega_0^2 x^2), \quad E_Y = \frac{1}{2}(\dot{y}^2 + \omega_0^2 y^2) \quad (26)$$

are the calculated energies of the  $x$ - and  $y$ -axis, respectively.

The other approach is to implement energy control scheme and estimate the damping terms of both axes independently. The energy control can be the same as that in Eq. (24), however, the amplitude of the energy control  $A$  is adjusted until the prescribed energy level is reached at both axes. Scalar versioned control laws of (13), (15) and (17) can be used to estimate  $d_x$  and  $d_y$ , thus damping ratio  $d_y/d_x$ .

These approaches are used at the initial calibration stage with the assumption of zero angular rate when the gyroscope is turned on, or at regular calibration sessions which may be performed periodically to identify the ratio. Once the ratio is identified, its value can be frozen until the next calibration session, because the variation of damping ratio is negligibly slow compared with damping itself.

Although a recently developed mechanically decoupled gyroscope structure has shown that the two axes can be mechanically decoupled to a great extent, there may be still a coupled stiffness term which comes mainly from misalignment of sensors and actuators. In this case, a coupling compensator is needed to compensate for the coupling effect in stiffness between the two axes at an initial calibration stage. A force balancing control [17] is used to compensate the coupling term so that it drives the  $y$ -axis output to and holds it at zero. It is given as a PI-type controller as follows.

$$\hat{\omega}_{xy} = \left( K_1 + \frac{K_2}{s} \right) \text{LPF}(y \cos \omega_0 t) \quad (27)$$

$$f_{xb} = \hat{\omega}_{xy} y$$

where  $f_{xb}$  is a force-balancing control, and  $K_1$  and  $K_2$  are the proportional and integral gains.

### 3.4. Rotation angle calculation

When the gyroscope is allowed to freely oscillate and controlled to compensate for damping, mismatched natural fre-

Table 1  
Parameters of the gyroscope and controller for the simulation

Parameter	Value
Gyroscope	$\omega_0 = 1$ ; $\omega_x = 1.05$ ; $\omega_y = 0.97$ ; $\omega_{xy} = 0.001$ ; $d_x = 0.05$ ; $d_y = 0.06$
Energy control	$K_P = 0.2$ ; $K_I = 0.002$
Mode tuning control	LPF = 0.5/s + 0.5; $K_{IM} = 0.0003$
Coupling compensator	$K_1 = 0.2$ ; $K_2 = 0.002$

quencies and coupled stiffness term until the operation of an ideal gyroscope is reached, the precession of the straight line of oscillation provides a measure of the rotation angle. The angle can be calculated from the measurement of the vector displacement:

$$\psi = -\tan^{-1} \left( \frac{\text{LPF}(y \sin \omega_0 t)}{\text{LPF}(x \sin \omega_0 t)} \right) - \psi_0 \quad (28)$$

where  $\psi_0$  is initial precession angle.

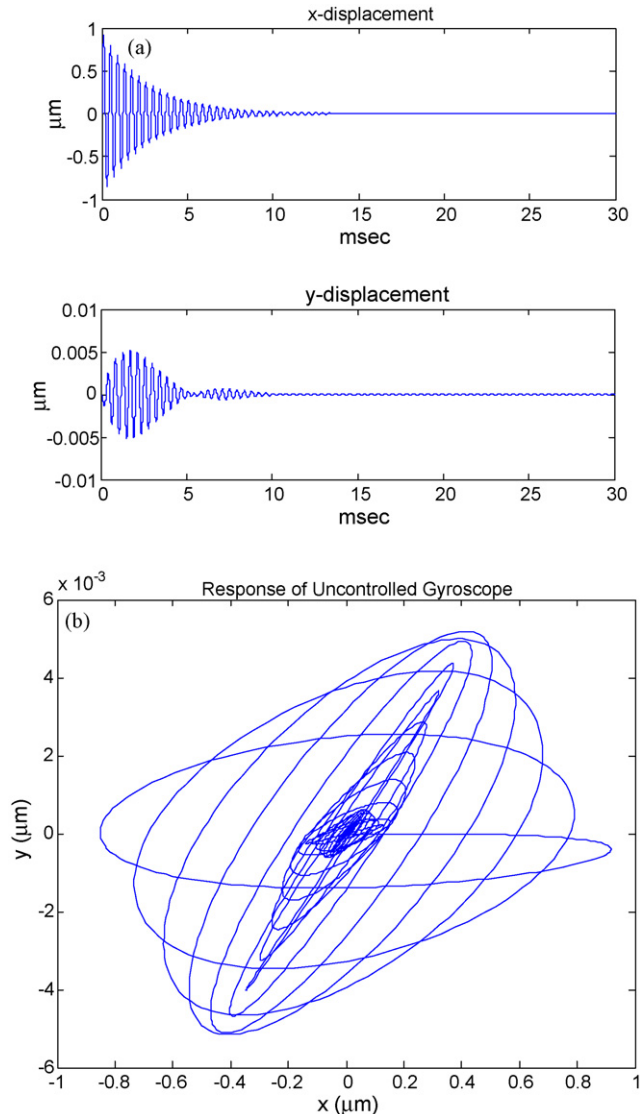


Fig. 2. Response of uncontrolled gyroscope: (a)  $x$  and  $y$  motion and (b) motion in  $x$ - $y$  plane.

The bandwidth of an angle measuring gyroscope is potentially unlimited because the overall system energy remains constant and the rotation angle is measured off the relative change in energy between the two orthogonal modes. In practice, if the resonant frequency is at least one order greater than the rotation rate, then the precession angle can track the input angular velocity exactly [10]. On the other hand, the bandwidth of the proposed controlled gyroscope is defined by the cut-off frequency of the low-pass filter used in this rotation angle calculation process.

#### 4. Simulation results

To evaluate the proposed control scheme, computer simulations are performed using a MEMS gyroscope model built at Sejong University. The specified reference natural

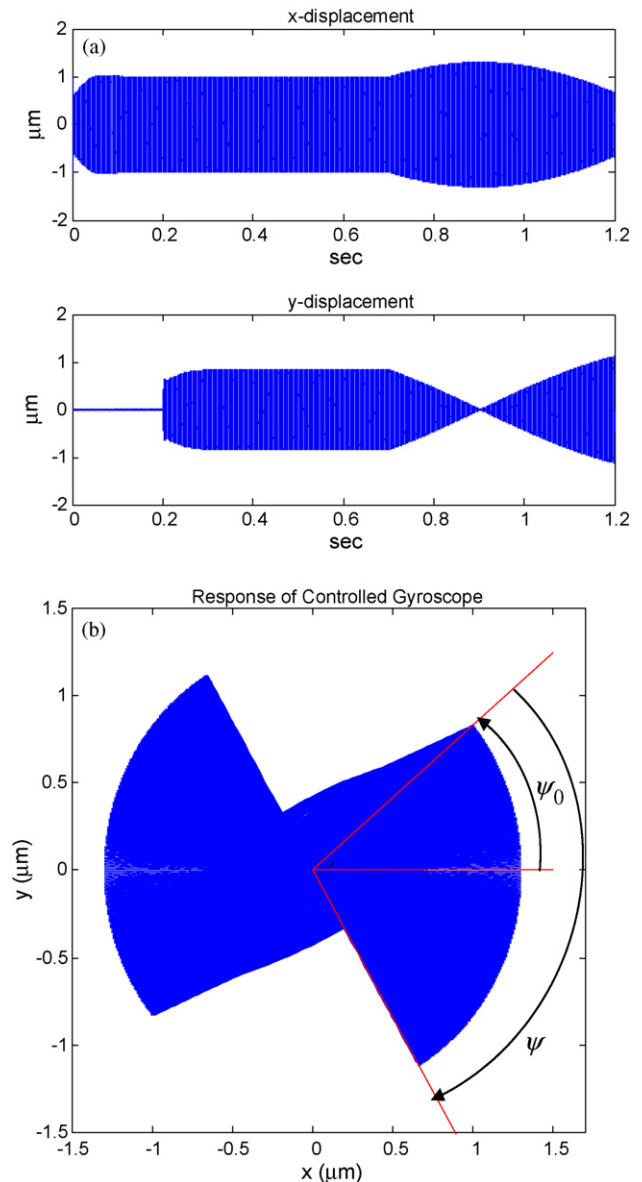


Fig. 3. Response of controlled gyroscope: (a)  $x$  and  $y$  motion and (b) motion in  $x$ - $y$  plane.

frequency is 2.3 kHz. We assumed that the natural frequencies of the  $x$ - and  $y$ -axis have 5% and 3% deviation errors from the reference frequency, respectively, and the magnitude of coupled frequency error is 0.1% of the reference frequency. The position and velocity measurements are contaminated by the electrical noise in the sensing circuit. The analysis of the stochastic properties of the measurement noise, as well as the estimation of their power spectral density (PSD), is given in Ref. [18]. In these simulations, both measurement noises are assumed to be zero-mean white with PSDs of  $4.35 \times 10^{-22} \text{ m}^2/\text{Hz}$  and  $2.3 \times 10^{-15} (\text{m s})^2/\text{Hz}$ , respectively. The gyroscope parameters in the model and the numerical values for the controller in the simulations are summarized in Table 1. Note that these values are shown in non-dimensional units, which are non-dimensionalized based

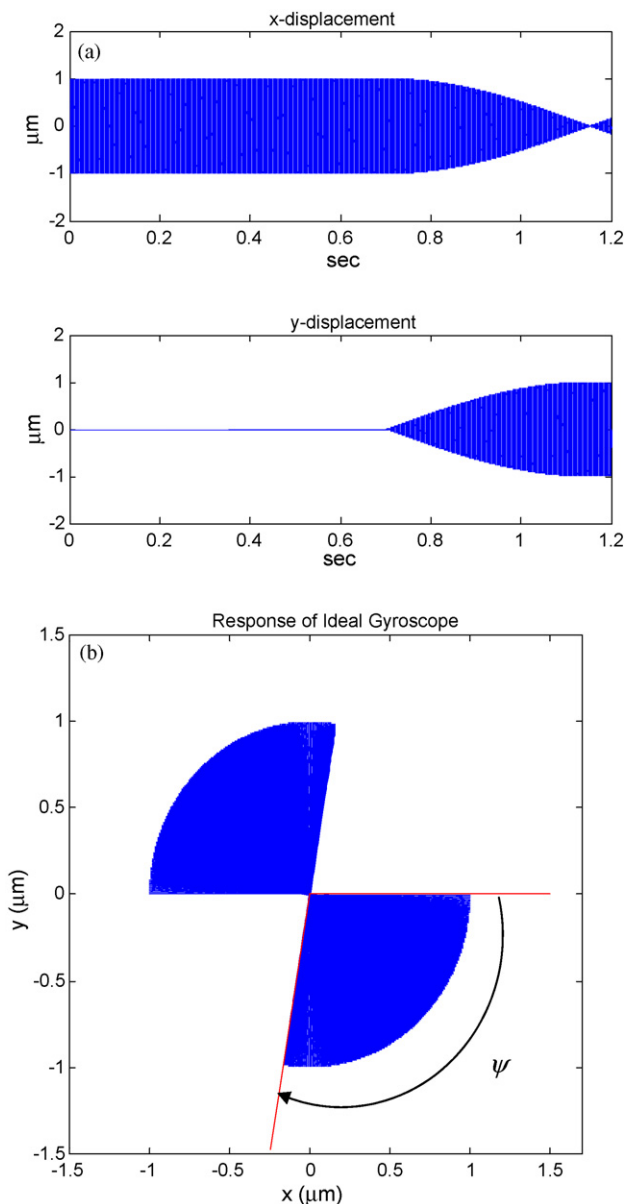


Fig. 4. Response of ideal gyroscope: (a)  $x$  and  $y$  motion and (b) motion in  $x$ - $y$  plane.

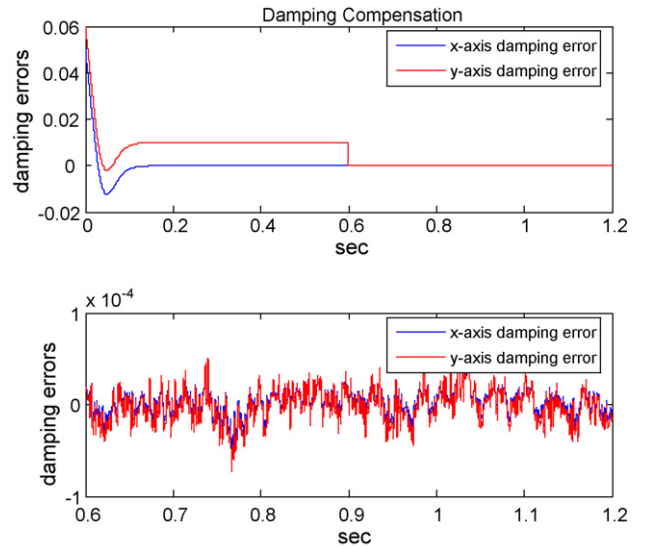


Fig. 5. Time response of estimation errors of damping terms.

on length of one-microns and the reference natural frequency.

Fig. 2 shows a simulation of the trajectory when the natural frequencies are not matched and there are unequal damping and frequency coupling in the gyroscope model. The straight line of oscillation is disrupted. Also the presence of damping results in energy dissipations and drives the free oscillations of the mass to zero. Fig. 3 shows that the proposed controller compensates for imperfections and makes the gyroscope behave like an ideal angle measuring gyroscope. The behavior of ideal gyroscope is also plotted in Fig. 4 and shows that the precession of the straight line of oscillation can provide a measure of the angle of rotation.

The time responses of the estimation errors for the various gyroscope parameters and the angle estimates obtained using the proposed controller are shown in Figs. 5–8. In these simu-

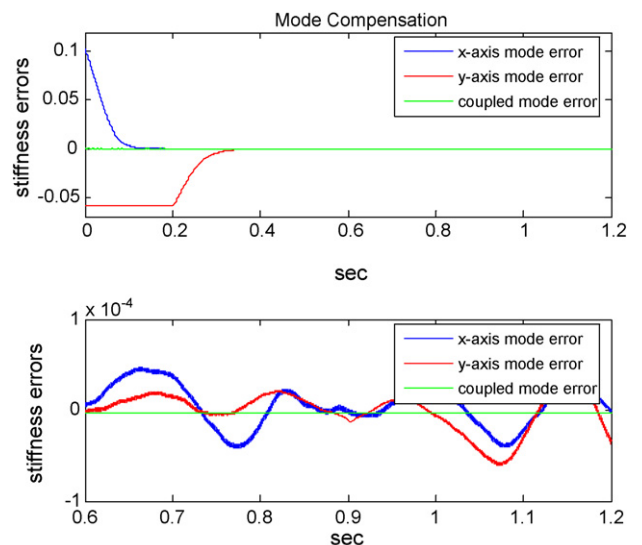


Fig. 6. Time response of estimation errors of frequency deviations.

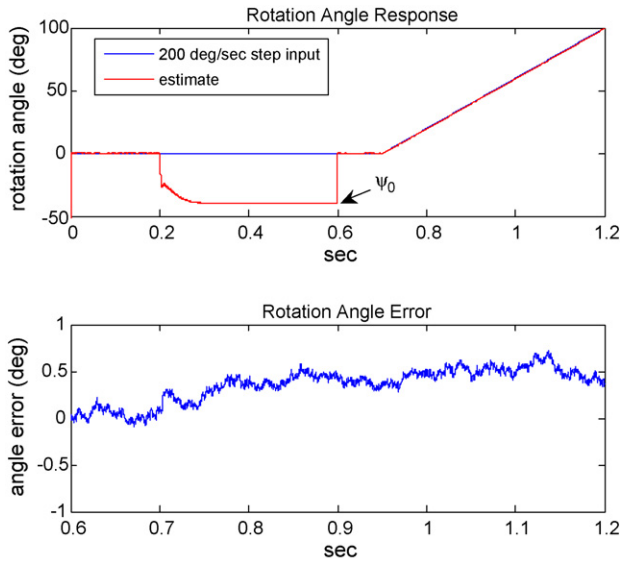


Fig. 7. Time response of rotation angle estimate to the 200°/s step input.

lations, the controller allows calibration period of 0.6 s and the gyroscope experiences a step input angular rate of 200°/s at 0.7 s after the gyroscope is turned on. The second plots in Figs. 5 and 6 show the influence of noise on the parameter estimations. The measurement noise limits its parameter estimation resolution and degrades overall gyroscope performance as shown in the second plots in Figs. 7 and 8. Detailed noise analysis, together with experimental results, will be presented in future publications. Fig. 8 shows the estimate of angle response to a sinusoidal input angular rate. According to the plots, the angle measuring accuracy with the error bound of 0.5° is achieved under the presence of noise. These simulation results clearly show that the proposed controller realizes angle measuring gyroscope operation successfully.

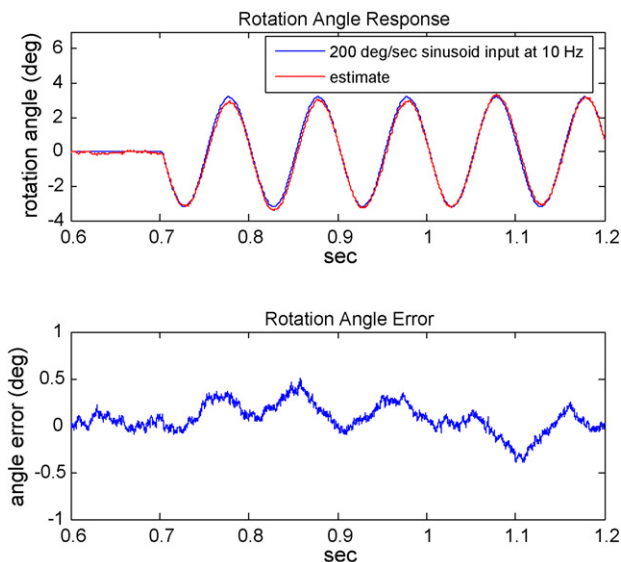


Fig. 8. Time response of rotation angle estimate to the 200°/s sinusoidal input at 10 Hz.

## 5. Conclusions

This paper presents a new control algorithm for realizing angle measuring gyroscopes. It consists of a weighted energy control, a mode tuning control, and an initial calibration stage. The developed control algorithm nulls out imperfections in MEMS gyroscopes such as mismatched stiffness, coupled stiffness and unequal damping term, and makes a non-ideal gyroscope behaves like an ideal gyroscope. It operates the gyroscope at a reference frequency, chosen by the designer, which results in control problem's easy and simple signal processing such as calculating total energy and demodulating the output signals.

The simulation studies show the feasibility and effectiveness of the developed algorithm that is capable of directly measuring rotation angle without the integration of angular rate.

The proposed algorithm can be applied to a conventional vibratory rate gyroscope structure, and realizes angle measuring operation by replacing the existing control algorithm to the proposed algorithm.

The control algorithm described in this paper, together with the necessary driving and sensing circuits, is currently being implemented for experiments. Results from these experiments will be presented in future publications.

## Acknowledgement

This work was supported by the Korea Research Foundation Grant funded by the Korean Government (KRF-2004-003-D00111).

## Appendix A

The proofs of Theorems 1 and 2 are provided in this appendix.

### A.1. Proof of Theorem 1

$\dot{V} \leq 0$  implies that  $V(t) \leq V(0)$  for  $t \geq 0$ . Thus,  $V$  is bounded. The derivative of  $\dot{V}$  is

$$\ddot{V} = -2K_P \tilde{E} \dot{\tilde{E}} \dot{q}^T \dot{q} - 2K_P \tilde{E}^2 \dot{q}^T \ddot{q}$$

This shows that  $\ddot{V}$  is bounded. Therefore, by Barbalat's lemma [15],  $\dot{V} \rightarrow 0$  or equivalently,  $\tilde{E} \rightarrow 0$ . Taking the derivative of  $\tilde{E}$  gives

$$\ddot{\tilde{E}} = -2\dot{q}^T (K_P \tilde{E} + \tilde{D}) \ddot{q} - \dot{q}^T (K_P \dot{\tilde{E}} + \dot{\tilde{D}}) \dot{q}$$

Thus,  $\ddot{\tilde{E}}$  is also bounded. Applying the Barbalat's lemma again gives

$$\dot{\tilde{E}} = -\dot{q}^T (K_P \tilde{E} + \tilde{D}) \dot{q} \rightarrow 0 \quad (29)$$

Since  $\tilde{E} \rightarrow 0$ , Eq. (29) implies that

$$\dot{q}^T \tilde{D} \dot{q} \rightarrow 0 \quad (30)$$

Therefore, if equal damping of both axes is assumed, i.e.  $\tilde{D} = \tilde{d}I$ , then  $\tilde{d} \rightarrow 0$  is guaranteed, where  $\tilde{d}$  is an equal damping estimate error, and  $I$  is an identity matrix.

## A.2. Proof of Theorem 2

Using the following PDF,

$$V = \frac{1}{2} \left( \tilde{E}^2 + \frac{1}{K_1} \tilde{\alpha}^2 \right) \quad (31)$$

and the steps same as those in proof of **Theorem 1**, one can easily show that as time  $t \rightarrow \infty$ ,  $\tilde{E} \rightarrow 0$ ,  $\dot{\tilde{E}} \rightarrow 0$ , and  $\tilde{\alpha} \rightarrow 0$ .

## References

- [1] N. Yazdi, F. Ayazi, K. Najafi, Micromachined inertial sensors, *Proc. IEEE* 86 (8) (1998) 1640–1659.
- [2] A. Lawrence, *Modern Inertial Technology*, Springer-Verlag, New York, 1998.
- [3] A. Shkel, R. Howe, R. Horowitz, Modeling and simulation of micromachined gyroscopes in the presence of imperfections, in: *Proceedings of the International Conference On Modeling and Simulation of Microsystems*, Puerto Rico, USA, 1999, pp. 605–608.
- [4] R. M'Closkey, A. Vakakis, Analysis of a microsensor automatic gain control loop, in: *Proceedings of the American Control Conference*, San Diego, CA, 1999, pp. 3307–3311.
- [5] R. Leland, Lyapunov-based adaptive control of a MEMS gyroscope, in: *Proceedings of the American Control Conference*, Vol. 3, 2002, pp. 3765–3770.
- [6] S. Park, *Adaptive control strategies for MEMS gyroscopes*, PhD Dissertation, U.C. Berkeley, 2000.
- [7] B. Friedland, M. Hutton, Theory and error analysis of vibrating-member gyroscopes, *IEEE Trans. Autom. Control* 23 (4) (1978) 545–556.
- [8] A. Shkel, R. Horowitz, A. Seshia, S. Park, R. Howe, Dynamics and control of micromachined gyroscopes, in: *Proceedings of the American Control Conference*, Vol. 3, 1999, pp. 2119–2124.
- [9] A. Shkel, R. Howe, micromachined angle measuring gyroscope, U.S. Patent 6,481,285 (2002).
- [10] C. Painter, A. Shkel, Detection of orientation and predicted performance of a MEMS absolute angle measuring gyroscope, in: *Proceedings of the 4th International Workshop on Structural Health Monitoring*, 2003, pp. 1011–1018.
- [11] C. Painter, A. Shkel, Experimental evaluation of a control system for an absolute angle measuring micromachined gyroscope, *IEEE Sens.* (2005) 1084–1087.
- [12] D. Piyabongkarn, R. Rajamani, M. Greminger, Development of a MEMS gyroscope for absolute angle measurement, *IEEE Trans. Control Syst. Technol.* 13 (2) (2005) 185–195.
- [13] S. Alper, T. Akin, A symmetric surface micromachined gyroscope with decoupled oscillation modes, *Sens. Actuators A: Phys.* 97–98 (2002) 347–358.
- [14] Y. Mochida, M. Tamura, K. Ohwada, A micromachined vibrating rate gyroscope with independent beams for the drive and detection modes, *Sens. Actuators A: Phys.* 80 (2000) 170–178.
- [15] J. Slotine, W. Li, *Applied Nonlinear Control*, Prentice Hall, Englewood Cliffs, 1991.
- [16] X. Sun, R. Horowitz, K. Komvopoulos, Stability and resolution analysis of a phase-locked loop natural frequency tracking system for MEMS fatigue testing, *IEEE J. Dyn. Syst. Measurement Control* 124 (4) (2002) 599–605.
- [17] X. Jiang, J. Seeger, M. Kraft, B. Boser, A monolithic surface micromachined z-axis gyroscope with digital output, in: *Symposium on VLSI Circuits*, Honolulu, HI, 2000, pp. 16–19.
- [18] B. Boser, Electronics for micromachined inertial sensors, in: *Proceedings of the International Conference on Solid-State Sensors and Actuators*, 1997, pp. 1169–1172.

## Biographies

**Sungsu Park** was born in Taejon, Korea in 1966. He received the BS and MS degrees in Aerospace Engineering from Seoul National University, Seoul, Korea in 1988 and 1990, respectively, and a PhD degree in Mechanical Engineering from the University of California at Berkeley in 2000. He is currently an associate professor of the Department of Aerospace Engineering of Sejong University, Seoul, Korea. His research interests include estimation theory, fuzzy control, adaptive and robust control with applications to micro-electro-mechanical systems (MEMS) and aerospace systems.

**Roberto Horowitz** was born in Caracas, Venezuela in 1955. He received a BSc Degree with Highest Honors in Mechanical Engineering from the University of California at Berkeley in 1978 and a PhD degree from the same institution in 1983. In 1982 he joined the Department of Mechanical Engineering of the University of California at Berkeley, where he is currently a Professor. Dr. Horowitz teaches and conducts research in the areas of adaptive, learning, nonlinear and optimal control with applications to micro-electro-mechanical systems (MEMS), mechatronics, robotics and intelligent vehicle and highway systems (IVHS). Dr. Horowitz was the recipient of a 1984 IBM Young Faculty Development Award and a 1987 NSF Presidential Young Investigator Award. He is a member of ASME and IEEE.

**Chin-Woo Tan** has been a Research Engineer with the California Partners for Advanced Transit and Highways (PATH) Program at the University of California, Berkeley since 1996. He was also a project manager at the same institution until late 2004. His research interests are in the areas of signal processing, estimation, navigation, intelligent transportation, bioengineering, and nonlinear dynamical systems. He has published in the areas of optimisation (pricing control), dynamical system (chaos), inertial navigation, and intelligent transportation. He has taught electrical engineering courses at U.C. Berkeley, U.C. Davis, and San Jose State University. Dr. Tan has a PhD in Electrical Engineering and a MA in Mathematics, both from U.C. Berkeley.